Journal of Power Sources 204 (2012) 60–66

Contents lists available at SciVerse ScienceDirect

Journal of Power Sources

journal homepage: www.elsevier.com/locate/jpowsour

Enhanced hydrogen generation from hydrolysis of $LiBH_4$ with diethyl ether addition for micro proton exchange membrane fuel cell application

Baicheng Weng*, Zhu Wu, Zhilin Li, Hui Yang

Shanghai Institute of Microsystem and Information Technology, Chinese Academy of Sciences, China

ARTICLE INFO

Article history:
Received 25 February 2011
Received in revised form 2 April 2011
Accepted 4 April 2011
Available online 5 January 2012

Keywords:
Lithium borohydride
Hydrolysis
Fuel cell
Hydrogen generation

ABSTRACT

$LiBH_4$ has a high hydrogen storage capacity and could potentially serve as a superior hydrogen storage material. However, in its hydrolysis process, incomplete hydrolysis caused by the agglomeration of $LiBH_4$ and its hydrolysis products limits its full utilization. In the present paper, a novel enhancement method to completely release the theoretical amount of hydrogen from $LiBH_4$ hydrolysis is presented by the addition of diethyl ether. The results show that in the presence of diethyl ether, hydrolysis of $LiBH_4$ can fully release 4 equivalents of hydrogen, and the agglomeration can be avoided. The enhanced performance can be attributed to the new phase $LiBH_4{\cdot}[Et_2O]_x$ which is formed through the combination of $LiBH_4$ with Et_2O molecules. Hydrolysis of this new phase shows a complete hydrolysis process with a slow kinetics. The method discussed in this paper presents a novel strategy to enhance the hydrolysis of borohydrides and other hydrides that have the same agglomeration problems. $LiBH_4$ diethyl ether suspension might be applied as a hydrogen generation source of micro proton exchange membrane fuel cells.

© 2012 Elsevier B.V. All rights reserved.

1. Introduction

Proton exchange membrane fuel cells (PEMFCs) are finding extensive use in applications ranging from small electronic devices to medium-sized stationary power generators [1–4]. To fuel the PEMFC, a hydrogen source is required. Taking both hydrogen related components and safety requirements into account, it is necessary to have a hydrolysable hydride with at least 10 wt.% hydrogen capacity [5].

Lithium borohydride ($LiBH_4$) has high gravimetric (18.5 wt.%) and volumetric (121 kg m^{-3}) capacities of hydrogen and can potentially serve as a good hydrogen storage material [6–13]. However, thermodynamic and kinetic limitations caused by strong covalent and ionic bonds greatly restrained the practical application of $LiBH_4$ as a reversible hydrogen storage material. In contrast, hydrolysis of $LiBH_4$ is of interest for the generation of hydrogen, because the theoretical hydrogen capacity of $LiBH_4$ hydrolysis is 13.9 wt.% (based on the weight of hydrides and the stoichiometric amount of water required) [14], which is higher than 8.9 wt.% for NH_3BH_3 hydrolysis [15] and 10.8 wt.% for $NaBH_4$ hydrolysis [16].

Previous studies have demonstrated that hydrolysis of $LiBH_4$ never produces more than 60% of its theoretical amount of hydrogen. Kojima et al. [14] found that the gravimetric and volumetric hydrogen densities increased with increasing $H_2O/LiBH_4$ ratio, and reached the maximum values of 7.4 wt.% and 60 kg m^{-3} at $H_2O/LiBH_4$ ratio of 3:1 (mol/mol), respectively. The hydrogen yield was only 50% of its theoretical value. Zhu et al. [17] also found the same results in their study and believed that the incomplete hydrolysis of $LiBH_4$ was attributed to $LiBH_4$ and its products forming a single solid and impermeable mass clogging the reaction vessel, thus limiting the full utilization of $LiBH_4$. In addition, they also showed that the hydrolysis kinetics of $LiBH_4$ was fast, *e.g.* at a very slow water injection rate of 10 μL h^{-1}, the hydrogen release rate was 6.8 mL min^{-1} g^{-1}. Through examining the behavior of $LiBH_4$ reacting with water steam, Matthews and co-workers [18] demonstrated that hydrolysis of $LiBH_4$ never produced more than 60% of its theoretical yield, because that the products and un-reacted $LiBH_4$ formed a single solid mass inside the reactor that was difficult to remove at the end of the experiment.

These studies have demonstrated that the incomplete hydrolysis is caused by the agglomeration of hydrolysis products and un-reacted $LiBH_4$. High hydrogen yield will be achieved if the agglomeration can be avoided.

In the present work, a novel strategy to fully hydrolyze $LiBH_4$ by the addition of diethyl ether (Et_2O) is presented. Choosing Et_2O as an additive is motivated by the fact that $LiBH_4$ can dissolve in diethyl ether [19], in which its hydrolysis products $LiBO_2$ cannot dissolve. In addition, because water is miscible with Et_2O, addition of Et_2O cannot cut off the contact of water with dissolved $LiBH_4$. It was hoped that the hydrolysis products could be easily separated from the dissolved $LiBH_4$, and thus their agglomeration could be avoided. The hydrolytic behavior of $LiBH_4$ with

* Corresponding author. Tel.: +86 21 62511070; fax: +86 21 32200534.
E-mail address: bcweng@mail.sim.ac.cn (B. Weng).

0378-7753/$ – see front matter © 2012 Elsevier B.V. All rights reserved.
doi:10.1016/j.jpowsour.2012.01.051

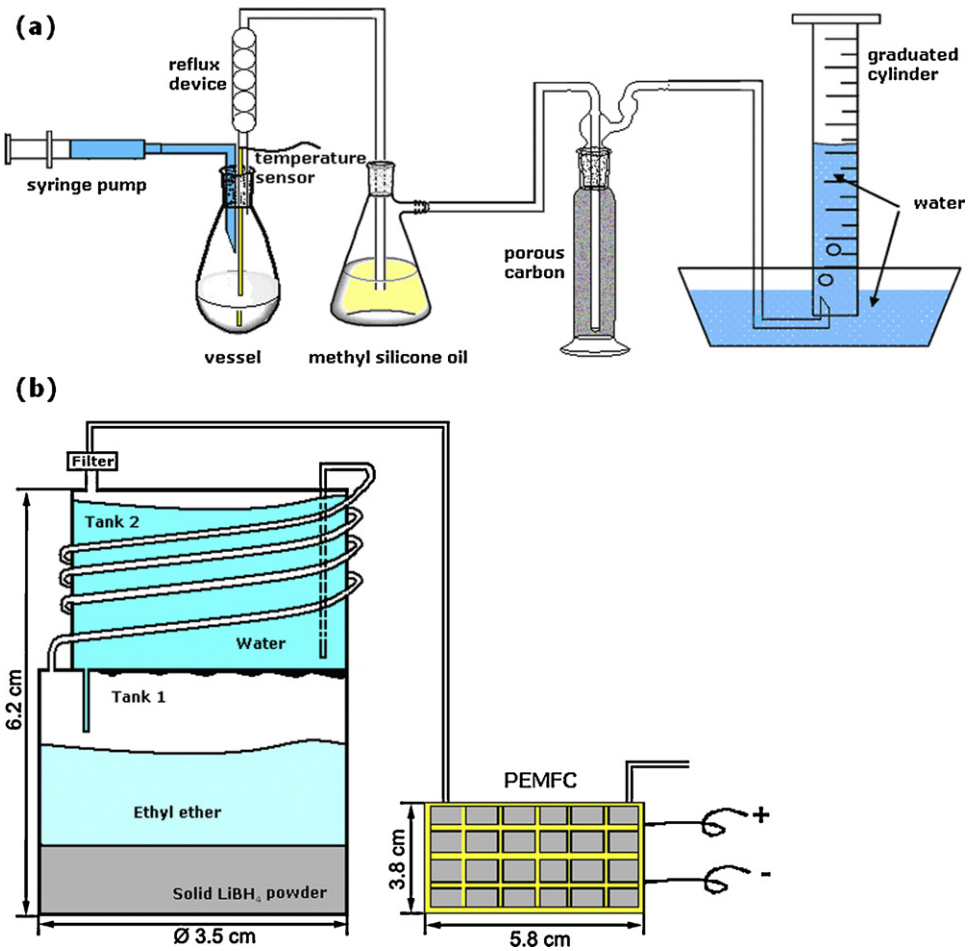

Fig. 1. Schematic plot of the experimental setup used to measure the hydrogen generation from $LiBH_4$ hydrolysis (a), and schematic plot of apparatus designed to test the performance of an air-breathing micro PEMFC driven by the hydrogen generated from hydrolysis of $LiBH_4$ Et_2O suspension (b).

Et_2O addition was examined in this paper. The potential mechanism for Et_2O addition was also discussed. Finally, a silicon-based micro electromechanical system (MEMS) PEMFC interconnected to a hydrogen generation reactor from hydrolysis of $LiBH_4$ Et_2O suspension. The performance of the PEMFC including polarization curve and power density plot are presented.

2. Experimental

2.1. Materials and characterizations

Lithium borohydride ($LiBH_4$, 95% purity) was purchased from Sigma–Aldrich. Diethyl ether (Et_2O, 99% purity) was purchased from Sinopharm Chemical Reagent Co., Ltd. All sample operations were conducted in an MBraun Labmaster 130 glove box maintained under argon atmosphere with <1 ppm O_2 and H_2O vapor.

X-ray diffraction (XRD) measurements were carried out by a Rigaku D/max 2400 diffractometer using Cu/Kα radiation. $LiBH_4$ Et_2O suspension was vacuumed to a paste-like mass which was coated on a 1 mm depth glass board and sealed with a polyvinylchloride (PVC) membrane to avoid oxidation during the XRD measurements. ^{11}B magic-angle-spinning nuclear magnetic resonance (MAS-NMR) experiments were carried out at room temperature on a Bruker Advance 300 NMR spectrometer (Bruker, Germany) operating at 9.7 T on 128.3 MHz. Spectra were obtained using a two-channel custom-built probe with a 3 mm ZrO_2 rotor, and the magic-angle-spinning rate was set to 5 kHz to avoid the overlapping of spinning sidebands on other resonance lines. 300 scans were taken for the samples. The chemical shifts were referenced to $NaBH_4$ (−41 ppm). Morphologies of hydrolysis products were characterized by a field emission scanning electron microscopy (FESEM, HITACHI S4700, Japan) at a 100 kV acceleration voltage. Ultraviolet-visible (UV) spectroscopy characterizations of plain Et_2O and $LiBH_4$ Et_2O solution were carried out using an EPP 2000C-100 spectrometer (Stellarnet, USA). Electrochemical characterizations were tested using a Solartron SI 1287 potentiostat (Solartron Analytical, Hampshire, UK).

2.2. Apparatus and procedures

A schematic diagram of the experimental setup used to measure the hydrogen generation is shown in Fig. 1a. The apparatus consisted of a small reaction vessel, a syringe pump, and a water trap. Reaction vessel is made of glass. It was designed for the reaction of $LiBH_4$ with liquid water. It was sealed by three plugs: a water inlet plug, a temperature sensor plug and a hydrogen outlet plug with a central hole covered with a reflux device, a methyl silicone oil filter and a porous carbon filter. The volume of the reaction vessel is 100 mL. The syringe pump was used to deliver water into the vessel to react with the hydrides. The generated gas was collected and its volume was measured in the water trap, which consisted of an inverted, water-filled 500 mL graduated cylinder immersed in a water tray, and interconnected with the reactor by polyvinylchloride tubing. The generated hydrogen was measured by graduated cylinder, and calculated according to the ideal gas equation referred to the molar value of $LiBH_4$ as 1 equivalent.

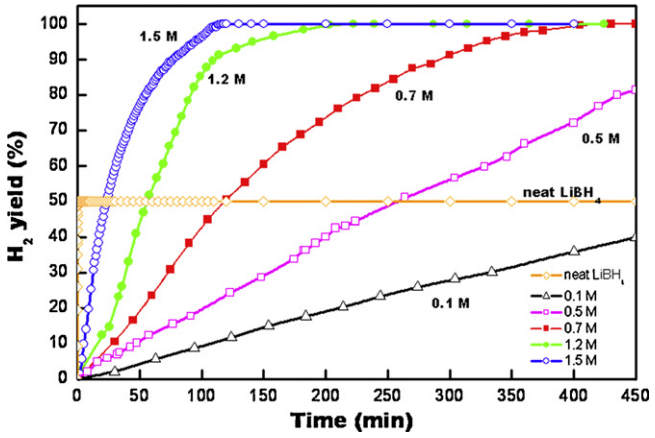

Fig. 2. Hydrogen yields as a function of time for hydrolysis of neat $LiBH_4$ and $LiBH_4$ Et_2O solutions ((◊) for neat $LiBH_4$, (△) for 0.1 M $LiBH_4$ Et_2O solution, (□) for 0.5 M, (■) for 0.7 M,(●) for 1.2 M and (○) for 1.5 M $LiBH_4$ Et_2O solution).

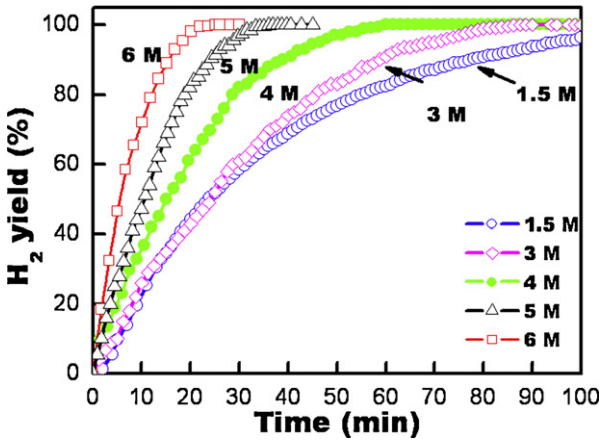

Fig. 3. Hydrogen yields as a function of time for hydrolysis of $LiBH_4$ Et_2O oversaturated suspensions ((○) for 1.5 M $LiBH_4$ Et_2O suspension, (◊) for 3 M, (●) for 4 M (△) for 5 M and (□) for 6 M $LiBH_4$ Et_2O suspension).

Fig. 1b shows an apparatus designed to test the performance of an air-breathing micro PEMFC supplied by the hydrogen generated from hydrolysis of $LiBH_4$ Et_2O suspension. This apparatus consisted of a device designed for generation hydrogen from $LiBH_4/Et_2O$ hydrolysis and a micro PEMFC interconnected with the device by PVC tubing. The volume of the hydrogen generator is 60 mL. It is comprised of two tanks (Fig. 1b). Tank 1 was filled with $LiBH_4$ powder, and on the top of the powder was $LiBH_4$ Et_2O solution. Tank 2 was filled with water. Driven by a differential pressure, water can drop into tank 1 through a tube. The volume of tank 1 is 48 mL. Its diameter is 3.5 cm, and its height is 5 cm. The volume of tank 2 is 12 mL, and its height is 1.2 cm. The initial amount of $LiBH_4$, Et_2O and water is 3 g, 22 g and 10 g, respectively. The PEMFC stack used in this paper is made with 6 individual fuel cells of 3.2 cm^2 each. It has the dimensions of 5.8 cm (length) × 3.8 cm (height) × 0.4 cm (thickness). Compared to the volume of the PEMFC stack (~9 mL), the volume of the hydrogen generator is not excessively large. Gas outlet of tank 1was connected with tank 2 by tubing, which circled around the exterior of tank 2 and plugged into the bottom of water in tank 2. This design aimed to reflux Et_2O back to tank 1. The gas outlet connected to the PEMFC was set on the top of tank 2 covered with a small porous carbon filter. The reflux and filter were designed to minimize the effect of Et_2O volatilization on the PEMFC.

3. Results and discussion

The hydrolysis reaction of $LiBH_4$ is [20]:

$$LiBH_4 + 2H_2O \rightarrow LiBO_2 + 4H_2 \quad (1)$$

Based on the weight of $LiBH_4$ and the stoichiometric amount of water required in Eq. (1), the total hydrogen capacity is 13.9 wt.%, which is higher than that of NH_3BH_3 hydrolysis (8.9 wt.%) [15], and $NaBH_4$ hydrolysis (10.8 wt.%) [16].

Fig. 2 compares the hydrogen generation profiles of neat $LiBH_4$ with $LiBH_4$ in Et_2O solution. As shown in Fig. 2, hydrolysis of neat $LiBH_4$ generates 50% of its theoretical amount of hydrogen (2055 mL g^{-1}) within 20 s. Hydrogen generation rate therefore corresponds to 6160 mL min^{-1} g^{-1}. Hydrolysis of neat $LiBH_4$ is not complete but its kinetics is fast. On the other hand, hydrogen generation rates from hydrolysis of $LiBH_4$ Et_2O solution are much slower. The rate is 3.6 mL min^{-1} g^{-1} for hydrolysis of 0.1 M $LiBH_4$ Et_2O solution, while the rate is 31 mL min^{-1} g^{-1} for hydrolysis of 1.5 M $LiBH_4$. Hydrogen generation rate increases with increasing concentrations of $LiBH_4$. The results show that in the presence of Et_2O, hydrogen release rate of $LiBH_4$ hydrolysis is greatly reduced.

When the concentration of $LiBH_4$ is higher than 0.7 M, the amount of hydrogen generated within 500 min is calculated by the ideal gas equation of state and found to be 3.8 equiv. which are the same as the theoretical value (3.8 equiv. hydrogen for 95% $LiBH_4$ hydrolysis) according to reaction (1). These results reveal that complete hydrolysis of $LiBH_4$ can be achieved and the agglomeration can be avoided by the addition of Et_2O.

In order to reduce the amount of Et_2O and increase the energy density of the $LiBH_4/Et_2O$ system, hydrolysis of $LiBH_4$ Et_2O oversaturated suspensions was investigated. The solubility of $LiBH_4$ in Et_2O is about 4.3 wt.% (~1.5 mol L^{-1}) at room temperature [19]. Fig. 3 shows the hydrogen generation profiles for hydrolysis of $LiBH_4$·Et_2O oversaturated suspensions with various $LiBH_4$ concentrations. As shown in Fig. 3, the hydrogen yields are 100% with the concentration of $LiBH_4$ ranging from 1.5 to 6 M. These results also reveal that the theoretical amount of hydrogen can be fully released from $LiBH_4/Et_2O$ solutions and suspensions. Hydrogen release rate increases from 31 to 160 mL min^{-1} g^{-1} with increasing concentrations of $LiBH_4$ from 1.5 to 6 M. Compared to $LiBH_4$ Et_2O solution (shown in Fig. 2), the hydrolysis rates of $LiBH_4$ oversaturated suspension are higher, but are still much lower than that of neat $LiBH_4$ hydrolysis.

Addition of Et_2O can reduce the contact rate between $LiBH_4$ and water by diluting water and $LiBH_4$. However, in the case of hydrolysis of 6 M $LiBH_4$ oversaturated suspension, although the amount of solid $LiBH_4$ is 2 times higher than the dissolved one, the hydrogen generation rate (160 mL min^{-1} g^{-1}) is still dramatically lower than that of neat $LiBH_4$ hydrolysis (6160 mL min^{-1} g^{-1}). In addition, the dependence of hydrogen generation rate on various amounts of Et_2O is not linear. These phenomena imply that $LiBH_4$ Et_2O suspension exhibits different hydrolysis properties from neat $LiBH_4$, and the dilution effect of Et_2O is not the main cause for the kinetic decrease. There is an extra effect of Et_2O besides the dilution effect discussed above.

Fig. 4 shows the maximum temperature profiles for hydrolysis of neat $LiBH_4$ and $LiBH_4$ Et_2O suspension. As shown in Fig. 4, hydrolysis of $LiBH_4$ is a high exothermic route. It can make the temperature of the vessel rise beyond 200 °C. In contrast, the temperature increments during hydrolysis of $LiBH_4$ Et_2O suspension do not exceed 12 °C, *i.e.* the maximum temperature reaches up to 31 °C during hydrolysis of 6 M $LiBH_4$ solution, and the temperature increment is only 4 °C during hydrolysis of saturated $LiBH_4$ solution (1.5 M). These results clearly show a different hydrolytic behavior

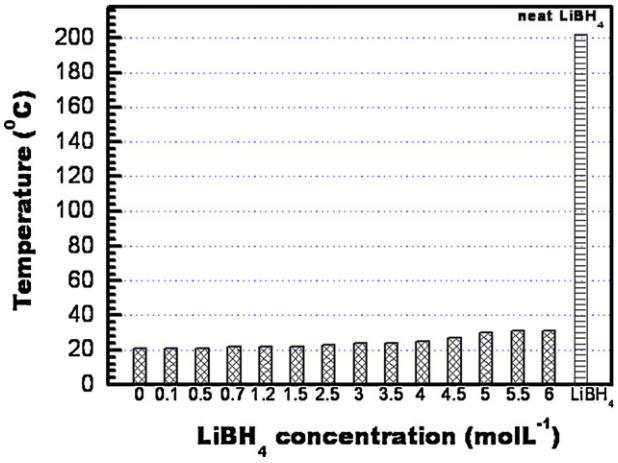

Fig. 4. Maximum temperature profiles for hydrolysis of neat $LiBH_4$ and $LiBH_4$ in Et_2O suspensions.

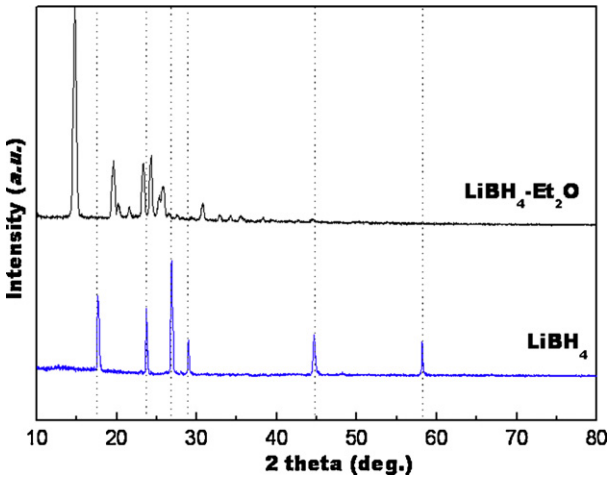

Fig. 6. XRD patterns of the neat $LiBH_4$ and $LiBH_4$ Et_2O suspension. The dashed line was added as a guide to the eye.

with the addition of Et_2O. In addition, the small temperature increment during hydrolysis of $LiBH_4$ saturated solution indicates that Et_2O would not severely volatilize during the hydrolysis process, coupled with the reflux and filter devices preventing the low amount of Et_2O escaping from the reactor, therefore the generated hydrogen purity will not be harshly decreased.

To clarify the potential structure changes after the addition of Et_2O, UV absorption spectra of neat Et_2O and $LiBH_4$ Et_2O solution are compared in Fig. 5. As shown in Fig. 5, the UV absorption position of Et_2O in the presence of $LiBH_4$ slightly shifts from 261 to 276 nm. Because there is no chemical reaction between Et_2O and $LiBH_4$, this result implies a weak bond between Et_2O and $LiBH_4$ molecules. XRD patterns of plain $LiBH_4$ and $LiBH_4$ Et_2O suspension are compared in Fig. 6. XRD results evidence the disappearance of $LiBH_4$ phase and the formation of new phases. We believe that the physical transformation of $LiBH_4$ phase results from the combination between Et_2O and $LiBH_4$ molecules forming a new phase $LiBH_4{\cdot}[Et_2O]_x$. Kolski et al. [19] have demonstrate that $LiBH_4$ and Et_2O can combine and form a new phase $LiBH_4{\cdot}[Et_2O]_x$, where x is dependent on the amount of Et_2O. Our results confirm Kolski's findings. Therefore, the hydrolysis reaction of $LiBH_4$ in Et_2O suspension can be described as follows:

$$LiBH_4{\cdot}[Et_2O]_x + 4H_2O \rightarrow LiBO_2{\cdot}2H_2O + 4H_2 + x\,Et_2O \quad (2)$$

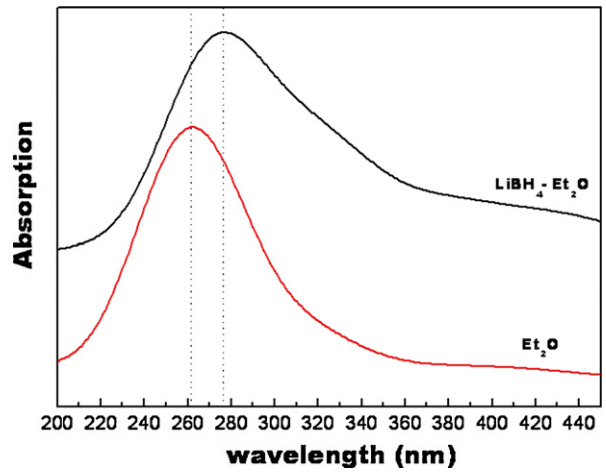

Fig. 5. UV absorption spectra of neat Et_2O (red line) and the $LiBH_4$ Et_2O solution (black line). The dashed line was added as a guide to the eye. (For interpretation of the references to color in this figure legend, the reader is referred to the web version of the article.)

$$LiBH_4\,(s) + x\,Et_2O \rightarrow LiBH_4{\cdot}[Et_2O]_x \quad (3)$$

The hydrolysis route is different from that of neat $LiBH_4$, resulting in a different hydrolysis performance. The weak combination between $LiBH_4$ and Et_2O greatly restrains the effective contact of $LiBH_4$ with water. It can explain the results that the kinetics is much slower than that of neat $LiBH_4$, and the reaction temperature remains low. Et_2O that is released from hydrolysis of $LiBH_4{\cdot}[Et_2O]_x$ shown in Eq. (2) can bond with un-reacted $LiBH_4$ to form $LiBH_4{\cdot}[Et_2O]_x$ again. Therefore, it can explain the "abnormally slow" kinetics of $LiBH_4/Et_2O$ suspension hydrolysis.

In addition, the decrease of the capacity caused by the addition of Et_2O could be minimized by increasing the content of $LiBH_4$ powder in the hydrolysis system described as follows. As shown in Fig. 1b, $LiBH_4$ Et_2O saturated solution is filled into the reactor to mix with $LiBH_4$ powder and then after the un-dissolved $LiBH_4$ depositing on the bottom, water is dropped in from the top to react with $LiBH_4$. The depleted $LiBH_4$ in the liquid can be continuously refilled by the un-dissolved $LiBH_4$ solid at the bottom (Eqs. (2) and (3)). Because Et_2O cannot be depleted during the hydrolysis process, increasing the amount of $LiBH_4$ powder leads to the hydrogen capacity increase. Moreover, because $LiBH_4$ in Et_2O suspension keeps stable for a long time, and the hydrogen generation rate is low, the gravimetric capacity loss caused by the addition of Et_2O can be offset by replacing the vessel material (stainless steel) with lighter plastic materials.

^{11}B NMR patterns of the condensed hydrolysis products of neat $LiBH_4$ and $LiBH_4$ Et_2O suspension are shown in Fig. 7. ^{11}B NMR characterization of the hydrolysis products of neat $LiBH_4$ shows 2 peaks at 1.8 ppm and −42 ppm, corresponding to $LiBO_2$ and un-reacted $LiBH_4$ [21–23]. The results demonstrate that hydrolysis of neat $LiBH_4$ is incomplete. On the other hand, there is no $LiBH_4$ peak for hydrolysis of $LiBH_4$ Et_2O suspension, the only observable peak at 1.8 ppm indicates the full hydrolysis of $LiBH_4$ achieved by the addition of Et_2O.

SEM images of the condensed products of neat $LiBH_4$ and $LiBH_4$ Et_2O suspension are compared in Fig. 8. No pores can be found on the surface of the neat $LiBH_4$ reaction products, the hydrolysis product of $LiBH_4$ is a single solid and impermeable mass. However, the product of $LiBH_4$ Et_2O suspension shows a porous morphology with low diameters of less than 10 μm, instead of forming an impermeable mass. The results confirm that the agglomeration is avoided by the addition of Et_2O.

Hydrolysis of $LiBH_4$ powder is a highly exothermic route with fast kinetics. During its hydrolysis process, hydrolysis of a large

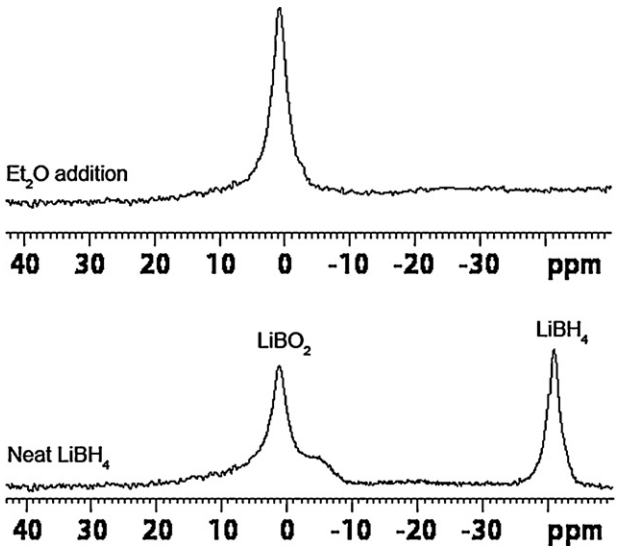

Fig. 7. ^{11}B NMR patterns of the condensed hydrolysis products of neat $LiBH_4$, and $LiBH_4$ Et_2O suspension.

amount of $LiBH_4$ accumulates a mass of heat, resulting in quick evaporation of water in the solid mass. In addition, the hydrolysis product $LiBO_2$ hydrates are impermeable solid mass. Therefore, the agglomeration prevents $LiBH_4$ in the solid mass reacting with water outside. Thus, $LiBH_4$ cannot fully release the theoretical amount of hydrogen. In contrast, in the hydrolysis process of hydrolysis of $LiBH_4$ with Et_2O addition, because the reaction temperature remains low, and the weak bond between Et_2O and $LiBH_4$ prevents the combination of $LiBH_4$ with $LiBO_2$ hydrates, the agglomeration of $LiBH_4$ with its products can be avoided.

Hydrogen generation device was connected to an air-breathing micro PEMFC self-made in our laboratory to test the fuel cell performance with the hydrogen generated from the hydride powder packed-bed reactor. The details of air-breathing micro-PEMFC have been reported in another paper [24]. When loaded with a current density of 200 mA cm^{-2}, the PEMFC needs only about 22 mL min^{-1} hydrogen, which is lower than the hydrogen generation rate for hydrolysis of saturated $LiBH_4$ Et_2O solution (31 mL min^{-1} g^{-1}). Therefore our hydrogen generator with a reasonable size can supply hydrogen for the PEMFC at adequate rates. The structure of the hybrid silicon fuel cell is depicted in Fig. 9. Briefly, the fuel cell was manufactured using MEMS fabrication processes. Beginning with a P-type silicon wafer polished on both sides, a 2 μm silicon dioxide layer was grown by wet thermal oxidation. Then photolithography was applied to define the flow channel geometry on the front side and the feed hole geometry on the rear side. The exposed oxide was removed by a buffered oxide etchant (BOE), followed by anisotropic KOH etching down to a channel depth of approximately 270 μm. After the residue of previously coated SiO_2 was removed by BOE, a new 2 μm silicon dioxide was grown as an insulator layer on the surface by wet thermal oxidation. Metal contact is made by sputtering gold. Nafion solution was painted to fill the channels with a paintbrush. A Pt-based catalyst ink was directly painted on the top of Nafion, and the resulting catalyst loading was approximately 20 mg cm^{-2}.

The polarization curve of the fuel cell supplied by hydrogen generated from reacting $LiBH_4$ with water is shown in Fig. 10, with open cell potential of 6 V and maximum power density of 0.1 W cm^{-2}. As shown in Fig. 11, the fuel cell stably ran at 150 mA cm^{-2} for 3 h supplied by the continuous hydrogen generated from $LiBH_4$ hydrolysis. When test time is longer than 3 h, the voltage decreases with time, which may result from the decrease of $LiBH_4$ concentration, as the reaction closes to end. The coulometric efficiency of our long-life test is 33%, which is lower than that of direct $NaBH_4$ fuel cells

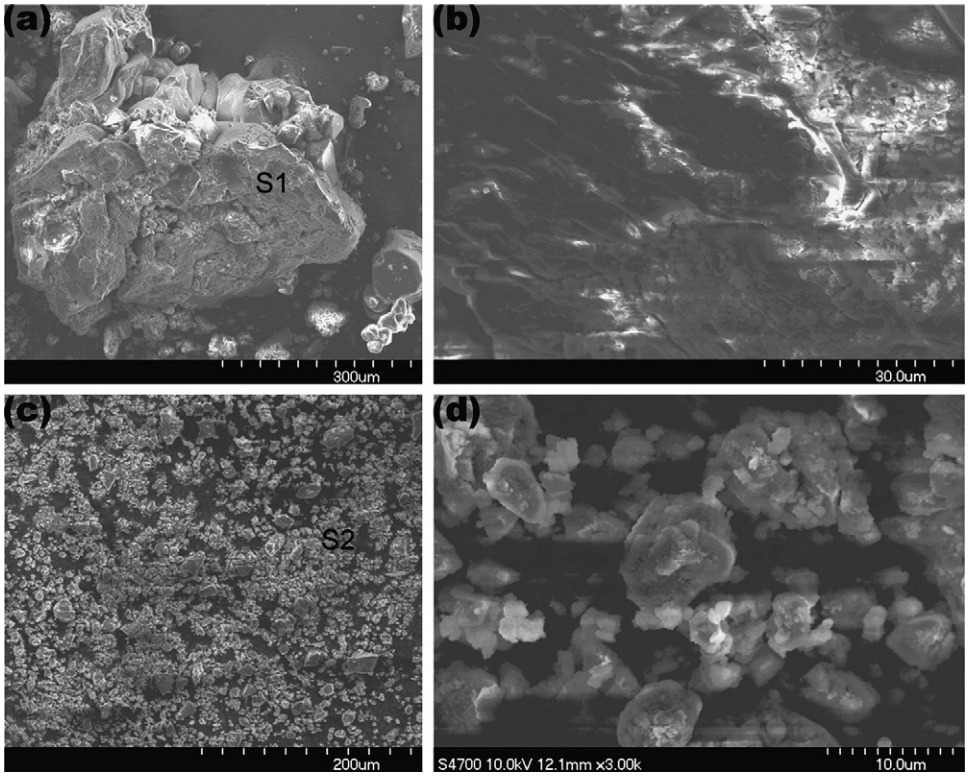

Fig. 8. SEM images of the condensed hydrolysis products of (a) neat $LiBH_4$, (b) amplified images of (a) S1 area, (c) $LiBH_4$ in Et_2O suspension and (d) amplified images of (c) S2 area.

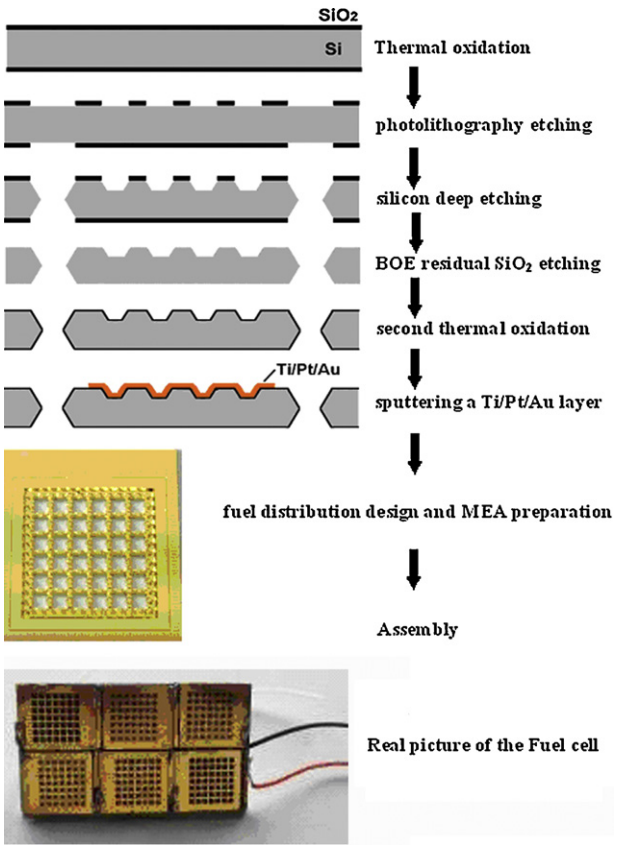

Fig. 9. Schematic plot of a MEMS micro silicon fuel cell.

[25–27] at the same current density. Different from direct borohydride fuel cells, our hydrogen source is connected to the PEMFC by PVC tubing. Therefore, in order to keep the fuel cell run steadily, the hydrogen generation rate must be higher than that required for the fuel cell, otherwise, the voltage of the fuel cell decreases continuously. In this case, a large amount of hydrogen that is vented out from the fuel cell cannot be utilized by the fuel cell, which is the cause for the low coulometric efficiency. The present work is only a fundamental study, and it aims to demonstrate that $LiBH_4$ can be 100% utilized to generate hydrogen, and the generated hydrogen can keep a PEMFC continuously working. Further work will focus on optimizing the system to achieve higher hydrogen utilization efficiency and achieve long-term long-life test by recycling the

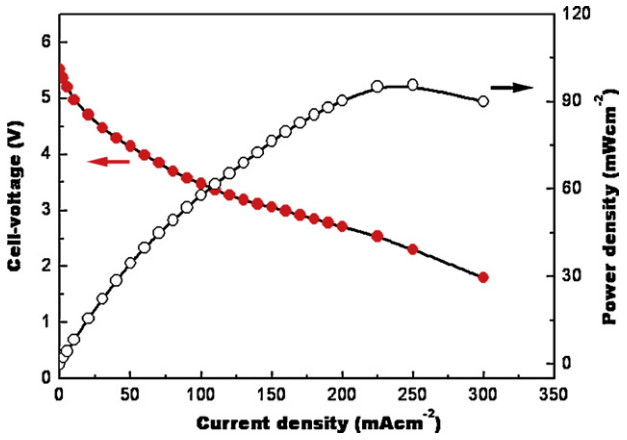

Fig. 10. Polarization curve of a micro-PEMFC with hydrogen generated from hydrolysis of $LiBH_4$ Et_2O suspension.

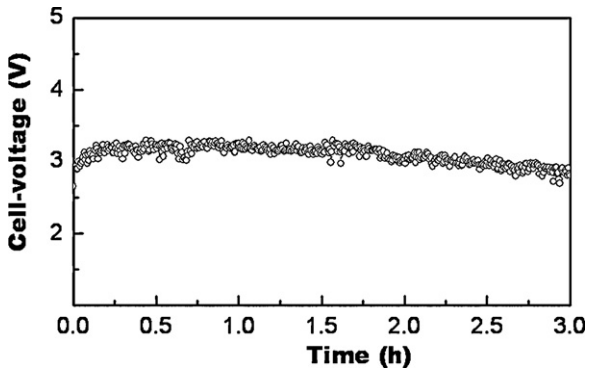

Fig. 11. Long-life test curve at 150 mA cm^{-2} of the FEMFC supplied by the hydrogen generated from hydrolysis of $LiBH_4$ Et_2O suspension.

hydrogen that is vented out from the fuel cell and stabilizing the hydrogen generation rate.

4. Conclusion

In summary, our results present a novel strategy for complete hydrolysis of $LiBH_4$ by the addition of Et_2O. It is shown experimentally that hydrolysis of $LiBH_4/Et_2O$ completely releases 4 equivalents of hydrogen at moderate rates. The agglomeration is avoided in the presence of Et_2O. The enhanced hydrolysis of $LiBH_4$ can be attributed to the combination of $LiBH_4$ with Et_2O molecules forming a new phase $LiBH_4{\cdot}[Et_2O]_x$. The hydrolysis route is the reaction of $LiBH_4{\cdot}[Et_2O]_x$ with water. This hydrolysis route is low exothermic, and its kinetics is slow. A fuel cell supplied by hydrolyzing $LiBH_4/Et_2O$ can stably run for 3 h, suggesting that $LiBH_4/Et_2O$ might be applied as a hydrogen generation source of proton exchange membrane fuel cells.

Acknowledgments

The authors would like to acknowledge the help of Fenghua Xu for revising our manuscript. This work was financially supported by National “863” High-Tech. Research Programs of China (2007AA05Z102, 2008AA05Z102 and 2007AA05Z149), Shanghai Natural Science Foundations (11ZR1444300 and 095SKA1001) and the SIMIT-QN Innovation Foundation (119900QN04).

References

[1] S.F.J. Flipsen, J. Power Sources 162 (2006) 927–934.
[2] Z.T. Xia, S.H. Chan, J. Power Sources 152 (2005) 46–49.
[3] J. Yeom, R.S. Jayashree, C. Rastogi, M.A. Shannon, P.J.A. Kenis, J. Power Sources 160 (2006) 1058–1064.
[4] W.M. Yang, S.K. Chou, C. Shu, J. Power Sources 164 (2007) 549–554.
[5] J. Yang, A. Sudik, D.J. Siegel, Angew. Chem. Int. Ed. 47 (2008) 882–887.
[6] L. Schlapbach, A. Züttel, Nature 414 (2001) 353–355.
[7] A. Züttel, P. Wenger, S. Rentsch, P. Sudan, Ph. Mauron, Ch. Emmenegger, J. Power Sources 118 (2003) 1–7.
[8] R.L. Cohen, J.H. Wernick, Science 214 (1981) 1081–1087.
[9] G.S. Walker, D.M. Grant, T.C. Price, X.B. Yu, V. Legrand, J. Power Sources 194 (2009) 1128–1134.
[10] H. Senoh, Z. Siroma, N. Fujiwara, K. Yasuda, J. Power Sources 185 (2008) 1–5.
[11] B.H. Liu, Z.P. Li, J. Power Sources 187 (2009) 527–534.
[12] J.J. Vajo, S.L. Skeith, J. Phys. Chem. B 109 (2005) 3719–3722.
[13] Y. Kojima, K. Suzuki, Y. Kawai, J. Power Sources 155 (2006) 325–328.
[14] Y. Kojima, Y. Kawai, M. Kimbara, H. Nakanishi, S. Matsumoto, Int. J. Hydrogen Energy 29 (2004) 1213–1217.
[15] M. Diwan, H.T. Hwang, A. Al-Kukhun, A. Varma, AIChE J. 57 (2011) 259–264.
[16] M.J.F. Ferreira, V.R. Fernandes, L. Gales, C.M. Rangel, A.M.F.R. Pinto, Int. J. Hydrogen Energy 35 (2010) 11456–11469.
[17] L. Zhu, D. Kim, H. Kim, R.I. Masel, M.A. Shannon, J. Power Sources 185 (2008) 1334–1339.
[18] R. Aiello, J.H. Sharp, M.A. Matthews, Int. J. Hydrogen Energy 24 (1999) 1123–1130.

[19] T.L. Kolski, H.B. Moore, L.E. Roth, K.J. Martin, G.W. Schaeffer, J. Am. Chem. Soc. 80 (1958) 549–552.
[20] B.C. Weng, Z. Wu, Z.L. Li, H. Yang, H.Y. Leng, J. Power Sources 196 (2011) 5095–5101.
[21] S.U. Jeong, R.K. Kim, E.A. Cho, H.J. Kim, S.W. Nam, I.H. Oh, S.A. Hong, S.H. Kim, J. Power Sources 144 (2005) 129–134.
[22] B.C. Weng, X.B. Yu, Z. Wu, Z.L. Li, T. Huang, N.X. Xu, J. Ni, J. Alloys Compd. 503 (2010) 345–349.
[23] M. Chandra, Q. Xu, J. Power Sources 156 (2006) 190–194.
[24] J.Y. Cao, Q.H. Huang, Z.Q. Zou, T. Yuan, Z.L. Li, B.J. Xia, H. Yang, J. Power Sources 185 (2008) 433–438.
[25] Z.P. Li, B.H. Liu, K. Arai, K. Asaba, S. Suda, J. Power Sources 126 (2004) 28–33.
[26] N.A. Choudhury, R.K. Raman, S. Sampath, A.K. Shukla, J. Power Sources 143 (2005) 1–8.
[27] L.B. Wang, C.N. Ma, Y.M. Sun, S. Suda, J. Alloys Compd. 391 (2005) 318–322.